minerals

MDPI

Article

First Direct Dating of Alteration of Paleo-Oil Pools Using Rubidium-Strontium Pyrite Geochronology

Shaojie Li [1], Xuan-Ce Wang [1,2,*], Chao-Feng Li [3], Keyu Liu [4,5], Simon A. Wilde [6], Si-Yu Hu [7], Lili Gui [8], Jianliang Liu [4] and Luya Wu [4]

[1] School of Earth Sciences, Yunnan University, Kunming 650500, China; shaojie.li1@postgrad.curtin.edu.au
[2] School of Earth and Environmental Sciences, The University of Queensland, Brisbane, QLD 4072, Australia
[3] State Key Laboratory of Lithospheric Evolution, Institute of Geology and Geophysics, Chinese Academy of Sciences, Beijing 100029, China; cfli@mail.iggcas.ac.cn
[4] School of Geosciences, China University of Petroleum, Qingdao 266555, China; liukeyu@upc.edu.cn (K.L.); 51liujianliang@163.com (J.L.); deyue123@163.com (L.W.)
[5] Laboratory for Marine Mineral Resources, Qingdao National Laboratory for Marine Science and Technology, Qingdao 266071, China
[6] The Institute for Geoscience Research (TIGeR), School of Earth and Planetary Sciences, Curtin University, Perth, WA 6845, Australia; S.Wilde@curtin.edu.au
[7] CSIRO Mineral Resources, Kensington, Western Australia 6151, Australia; siyu.hu@csiro.au
[8] Research Institute of Petroleum Exploration and development, PetroChina, Beijing 100083, China; gll@petrochina.com.cn
* Correspondence: x.wang4@uq.edu.au

Received: 11 May 2020; Accepted: 3 July 2020; Published: 4 July 2020

Abstract: Direct dating of petroleum systems by hydrocarbon or associated authigenic minerals is crucial for petroleum system analysis and hydrocarbon exploration. The precipitation of authigenic pyrite in petroliferous basins is commonly genetically associated with hydrocarbon generation, migration, accumulation, or destruction. Pyrite rubidium-strontium (Rb-Sr) isotope dilution thermal ionization mass spectrometry (ID-TIMS) is a well-developed technique, and its successful application for high-temperature ore systems suggests that this dating method has the potential to directly date key processes in the low-temperature petroleum systems. Rb-Sr data for pyrites in two Ordovician carbonate rock specimens collected from ~4952 m in the YD-2 well in the Yudong region, northern Tarim Basin (NW China), yield two identical isochron ages within analytical uncertainties: 206 ± 13 (2σ) and 224 ± 28 Ma (2σ). SEM investigations demonstrate that Rb and Sr atoms mainly reside in the crystal lattice of the pyrites due to the absence of fluid and mineral inclusions. The rigorous Rb-Sr isochron relations documented in the samples indicate that such residency can result in sufficient Rb/Sr fractionation and initial Sr isotopic homogenization for geochronology. In addition, the closure temperature (227–320 °C) for the Rb-Sr isotope system in pyrite is higher than the precipitation temperature for pyrite in petroleum-related environments (below 200 °C), suggesting that the Rb-Sr age of pyrite was not overprinted by post-precipitation alteration. Integrating the lead-strontium-sulfur isotopes of the pyrites with burial history analysis, the ages are interpreted as the timing of alteration of the paleo-oil pool by a hydrothermally-triggered thermochemical sulfate reduction process. This study, for the first time, demonstrates that Rb-Sr pyrite geochronology, combined with radiogenic and stable isotopic analyses, can be a useful tool to evaluate the temporal evolution of oil pools. This approach bears great potential for dating of petroleum systems anywhere else in the world.

Keywords: Rb-Sr pyrite geochronology; pyrite Pb-Sr-S isotope; Ordovician paleo-oil pool; Kuqa Depression; Tarim Basin

1. Introduction

Establishing the absolute timing for key events in petroleum systems (e.g., petroleum generation, charge and alteration) is crucial for petroleum system analysis and hydrocarbon exploration, but is still poorly constrained. Recent studies have demonstrated that isotope chronometers in hydrocarbons or associated minerals can be used for direct dating of petroleum generation and post-generation events [1,2]. For example, rhenium-osmium (Re-Os) isotopic analysis of petroleum samples can yield isochron ages approximating the timing of petroleum generation; however, the ages often have large errors [1]. Authigenic minerals, such as clays, which are precipitated and associated with petroleum may also be datable targets because radioactive atoms (e.g., potassium (K), rubidium (Rb)) can be incorporated into the minerals during their growth [2]. In addition, authigenic minerals usually have a genesis not as complex as petroleum, which is a hydrocarbon mixture generated by multiple source rocks or multi-stage generation processes. The genesis of authigenic minerals can be determined by radiogenic or stable isotopic analysis, enabling the unambiguous interpretation of the age data [3]. Therefore, more geochronological investigations on petroleum-related authigenic minerals are required in order to obtain high-precision age data for petroleum system analysis and exploration targeting.

Authigenic pyrite is a ubiquitous mineral in petroliferous basins and is commonly associated with the deposition of the source rock [4], hydrocarbon generation/expulsion [5], secondary migration/charge [6], and post-accumulation alteration [7]. Trace element systematics of pyrites are directly related to the depositional environment, such as water body, hydrothermal system and organic-inorganic fluid [8–10]. Therefore, the preserved metallic radiometric isotopic systems, such as rubidium-strontium (Rb-Sr) and lead (Pb), in authigenic pyrites, have the potential to serve as a chronometer and source-indicator, similar to that in well documented high-temperature ore deposits [3]. The sensitive isotope-dilution thermal ionization mass spectrometry (ID-TIMS) and low blank Rb-Sr separation/purification techniques developed in our laboratory permit high-precision Rb-Sr isotopic analysis of very small sample sizes [11,12]. In contrast to the large amount of sample used in conventional techniques (>100 mg for each analysis) [3], only 2–6 mg (average 3 mg) of pyrite was used in this study. This allows us to address sample heterogeneity by working directly on small sub-samples, and avoid the mixing problem present when utilizing the conventional ID-TIMS method that uses a much larger amounts of material, thus masking any fine-scale heterogeneity and hampering generating a meaningful isochron age. Therefore, theoretically, Rb-Sr pyrite geochronology should have the potential to date key processes in petroleum systems.

Pyrite is widely distributed in Ordovician hydrocarbon-bearing carbonate rocks within the Tarim Basin, North West (NW) China, and the precipitation of pyrite is closely associated with hydrocarbons [13–19]. Previous petrographic and isotopic studies have shown that there are two groups of pyrite; these are (i) by-products of thermochemical sulfate reduction (TSR) and (ii) bacterial sulfate reduction (BSR), respectively [13–19]. Sulfate minerals can be reduced to hydrogen sulfide (H_2S) by hydrocarbons either through bacterial metabolism (i.e., BSR) or thermochemical pathway (i.e., TSR) [7]. H_2S can be further transformed into pyrite provided there is a sufficient iron budget [7]. BSR-derived pyrites mainly occur in karst breccias and are characterized by depleted $\delta^{34}S$ values ranging from −25.7‰ to −4.7‰ in the Tarim Basin [14,16–19]. Those pyrites are precipitated in a low-temperature environment (60–80 °C) when hydrocarbon reservoirs are uplifted to the surface/subsurface [18,19]. TSR-derived pyrites mainly occur in fractures of the reservoir or coexist with other hydrothermal minerals (e.g., calcite) [18–20]. Pyrites of TSR origin have more enriched $\delta^{34}S$ values that are distributed between +11.2‰ and +31.3‰ in the Tarim Basin [13,15,18,19]. TSR requires a higher temperature environment (100–180 °C) compared to BSR [7]. The TSR process in the Tarim Basin is profoundly influenced by magmatism and associated hydrothermal activities that created a high-temperature environment and facilitated TSR [18–20].

The Yudong region is a significant petroleum exploration province in the Kuqa Depression, northern Tarim Basin (Figure 1). Here, Ordovician carbonate rocks are reservoirs for hydrocarbons generated from Cambrian-Ordovician marine source rocks [21]. YD-2 is the only well so far drilled into Ordovician-hosted hydrocarbons in the Yudong region, but limited heavy oil of uncommercial

value (~0.2 m^3/d) has been recovered from the interval between 4945 m and 4983.5 m during the formation test of the Ordovician strata [22]. Pyrite is commonly disseminated in the Ordovician oil-bearing interval in the drillhole YD-2 (Figure 2). This, therefore, provides a valuable opportunity to test the applicability of Rb-Sr pyrite geochronology to petroleum systems.

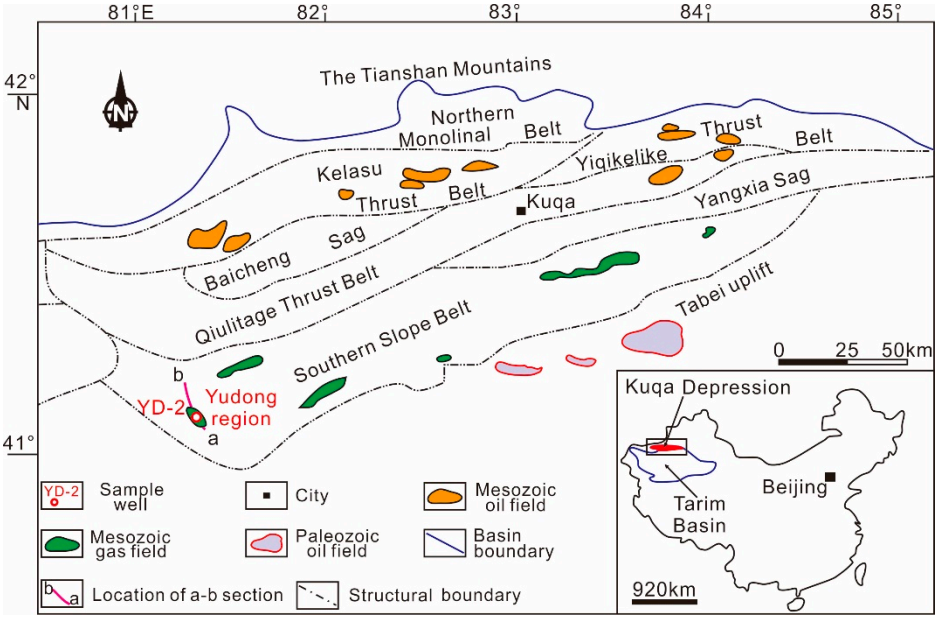

Figure 1. Drillhole YD-2 is located in the Southern Slope Belt of the Kuqa Depression in the Tarim Basin, NW China. The inset shows the locations of the Kuqa Depression and the Tarim Basin in China. (modified after [23]).

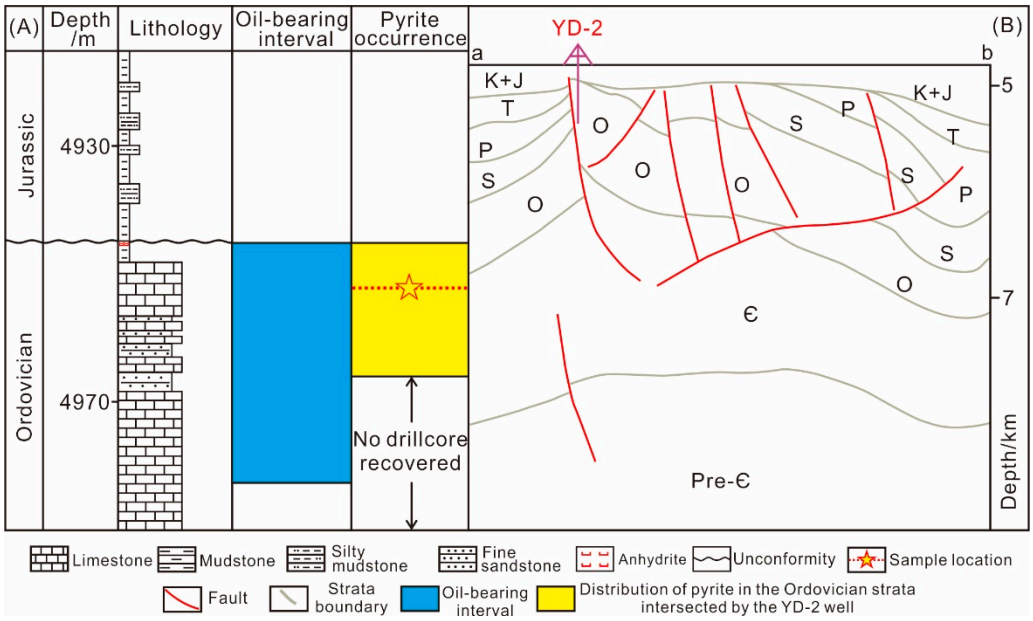

Figure 2. (**A**): In YD-2, the Ordovician strata are directly overlain by Jurassic strata. Limited amounts of heavy oil have been obtained from the Ordovician strata (4945 m and 4983.5 m) in YD-2. Pyrite is commonly disseminated in the oil-bearing interval [22]. (**B**): Nearby faults can be significant conduits for the migration of both hydrocarbons and hydrothermal fluids that are necessary for the precipitation of pyrite in the Ordovician reservoir of the YD-2 well. The location of the cross-section is shown in Figure 1. Є—Cambrian; O—Ordovician; S—Silurian; P—Permian; T—Triassic; J—Jurassic; K—Cretaceous.

2. Geological Background

The Kuqa Depression is situated in the northern part of the Tarim Basin, northwest (NW) China, and consists of seven structural units (Northern Monolinal Belt, Kelasu Thrust Belt, Yiqikelike Thrust Belt, Baicheng Sag, Qiulitage Thrust Belt, Yangxia Sag and Southern Slope Belt, Figure 1). The Yudong region lies in the Southern Slope Belt of the Kuqa Depression (Figure 1) and consists of Paleozoic-Cenozoic sediments [23]. Three major tectonic events have affected the Kuqa Depression: (1) a peripheral foreland basin stage (late Permian to Middle Triassic), (2) a rift basin stage (Late Triassic to Middle Jurassic), and (3) a rejuvenated foreland basin stage (early Neogene to the present-day) [23]. In YD-2, the Lower Ordovician is directly overlain by Jurassic strata (Figure 2A), indicating the Middle Ordovician to Triassic rocks have been eroded during the multi-stage tectonic movements that affected this region [24].

Ordovician hydrocarbon reservoirs in the Tarim Basin are significantly influenced by magmatism and associated hydrothermal activity [18–20]. Hydrothermal activity resulted in the precipitation of minerals such as calcite, and it created a high-temperature environment that was favorable for the occurrence of TSR in the reservoirs [13–19]. TSR is an important process for the formation of pyrite in the Ordovician reservoirs, and pyrites of TSR genesis are characterized by enriched sulfur isotope compositions [13,15,18,19]. In addition to TSR-derived pyrites, there are also pyrites precipitated under low-temperature conditions [18,19]. These pyrites have depleted sulfur isotope compositions and were formed by bacterial sulfate reduction [14,16–19].

3. Samples and Analytical Method

Pyrite samples analyzed in this study were separated from two pyrite-rich core specimens (A and B) taken at ~4952 m in the YD-2 well (Figure 2A). The samples were prepared as thin sections. Stereo binocular microscopy and scanning electron microscope-energy-dispersive X-ray spectroscopy (SEM-EDS, 200 kV, Zeiss Ultra plus Field Emission SEM at CSIRO) were employed to investigate the petrographic features of the samples.

Pyrite was separated by crushing the specimens in a porcelain mortar, followed by gravity sorting, electromagnetic separation and hand-picking under a binocular microscope. The obtained pyrite separates were cleaned with Milli-Q water and analytical-grade ethanol to further improve their purity and remove any contamination introduced by the mineral separation process. The two separate pyrite samples were prepared and dried completely on a hotplate prior to undertaking the chemistry.

Pyrite sub-samples were randomly picked from each sample so that they would potentially have a more homogeneous initial $^{87}Sr/^{86}Sr$ ratio (Sr_i). Each sub-sample was weighed (2–6 mg) using an AG104 Mettler Toledo analytical balance for Rb-Sr-Pb isotopic analyses and dissolved along with ^{87}Rb-^{84}Sr isotopic tracers in 14 N HNO_3 (~0.1 mL) in screw-top PFA Savillex vials. Rubidium, strontium, and lead fractions of each sub-sample were separated and purified using a mini-column containing ~30 μL of Sr Spec resin [12]. Isotope ratios of Rb and Sr were determined using ID-TIMS on a multi-collector Triton plus instrument at the State Key Laboratory of Lithospheric Evolution, Institute of Geology and Geophysics, Chinese Academy of Sciences (IGGCAS) in Beijing [12,25]. Lead isotope ratios were also measured by TIMS using the same instrument. $^{87}Sr/^{86}Sr$ ratios were normalized to $^{88}Sr/^{86}Sr = 8.375209$ [12,25] using the exponential law. Approximately 2 ng of the standard NBS 987 was loaded onto the filament and analyzed during the course of study, yielding a mean $^{87}Sr/^{86}Sr$ value of 0.710244 ± 0.000012 (2σ, n = 4) in good agreement with the reported values (0.710241–0.710255) [12,25,26]. Analytical uncertainties for $^{87}Rb/^{86}Sr$ ratios were less than 1%. The blank during the analytical session was less than 3 pg for Rb, 6 pg for Sr and 100 pg for Pb. Therefore, the contribution of total blank on the Rb-Sr and Pb isotopes can be ignored. In addition, based on the highly sensitive TaF5 emitter, we obtained strong signal intensity for Sr (~3000 mV of 88Sr), even for 2 ng sample size during TIMS measurements. This technique yielded a good precision (≤0.000039) for $^{87}Sr/^{86}Sr$ in this study. Rb-Sr isochron ages of pyrites were calculated using the ISOPLOT 3.0 software [27], applying a decay constant ($\lambda^{87}Rb$) of 1.42×10^{-11} yr^{-1} [28]. For Pb isotopes, in-run precision of individual analyses was better than 0.02% (2 RSE). Acids used during the Rb-Sr-Pb chemistry were

all analytical reagent (AR) grade and were purified utilizing a SavillexTM DST-1000 sub-boiling distillation system. Ultrapure water with resistivity of 18.2 MΩ.cm^{-1} obtained from a Milli-Q Element system was used throughout this work.

Sulfur isotopic ratios of pyrites (25–50 mg for each) were measured by a Finnigan MAT 252 mass spectrometer using the dual inlet method at IGGCAS. Sulfur has four stable isotopes (^{32}S, ^{33}S, ^{34}S and ^{35}S), and the fractionation of ^{34}S/^{32}S ratio can be observed in low-temperature settings. The sulfur isotope data are expressed in δ notion relative to Vienna Canyon Diablo Troilite (VCDT). i.e., $\delta^{34}S = ((^{34}S/^{32}S)_{sample}/(^{34}S/^{32}S)_{VCDT} - 1) \times 1000‰$. Two duplicate analyses were conducted for each sample (reproducibility of δ^{34}S value is ±0.1 − 0.3‰.). Analytical precision for δ^{34}S values of the duplicate analyses of IAEA standards (IAEA-S1 (−0.2‰), IAEA-S2 (22.10‰) and IAEA-S3(−32.53‰)) was better than ±0.1‰ (1σ, SD).

4. Results

4.1. Petrographic Observations

Pyrite crystals were characterized by using both stereo binocular microscope photomicrographs (Figure 3A,B) and scanning electron microscope-energy-dispersive X-ray spectroscopy (SEM-EDS) images (Figure 4A–I). SEM images illustrate that pyrite, calcite and quartz are intergrown and show embayment structures (Figure 4A), suggesting that these minerals were precipitated contemporaneously from hydrothermal fluids which may have migrated along faults near the YD-2 well (Figure 2B). The coexistence of pyrite and bitumen was also observed in this study (Figure 3B), which indicates that the formation of pyrite in the sampled reservoir rock may be the result of the interaction between hydrocarbon and hydrothermal fluid.

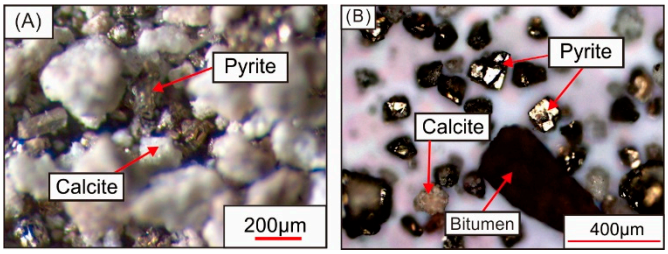

Figure 3. Typical stereo binocular microscope photomicrographs (reflective light) show that pyrites are disseminated in the samples and coexist with calcites in specimen A (**A**), with bitumen are found to coexist with pyrite and calcite in specimen B (**B**).

The high-resolution SEM images show that pyrites in this study contain no mineral or fluid inclusions (Figure 4B–I). Furthermore, potassium elemental mapping of pyrite indicates that the K content is below the detection limit of the instrument (Figure 5A–H). The lack of K also indicates the absence of K-bearing inclusions that might also accommodate Rb.

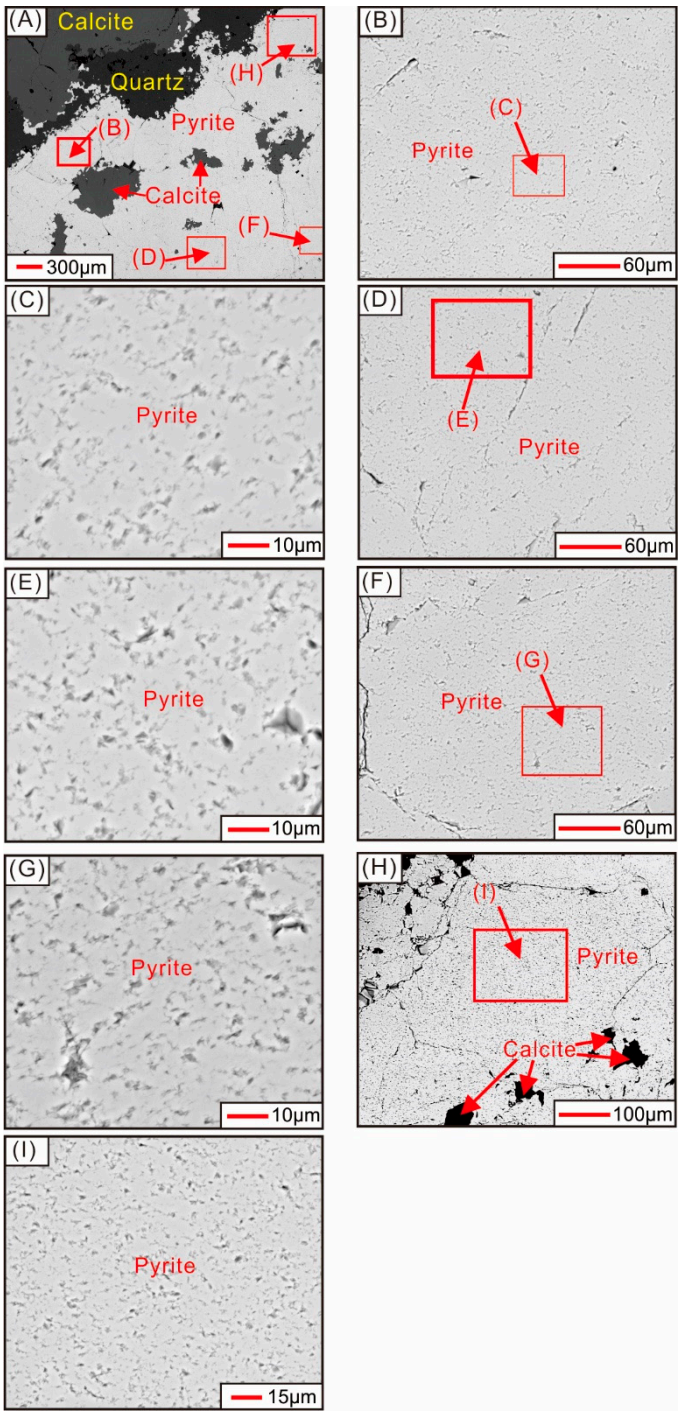

Figure 4. A typical SEM image of a thin section (**A**) shows the embayment structures between pyrite, calcite and quartz, suggesting that these minerals were precipitated contemporaneously from the hydrothermal fluid. High resolution SEM images (**B**–**I**) show that pyrites in this study are quite clean and free from mineral or fluid inclusions, suggesting that Rb and Sr mainly reside in the mineral lattices. (**B**,**D**,**F**,**H**) show the enlarged regions in (**A**). (**C**,**E**,**G**,**I**) show the enlarged regions in the (**B**,**D**,**F**,**H**), respectively. Locations of the enlarged regions are labelled in the corresponding figures.

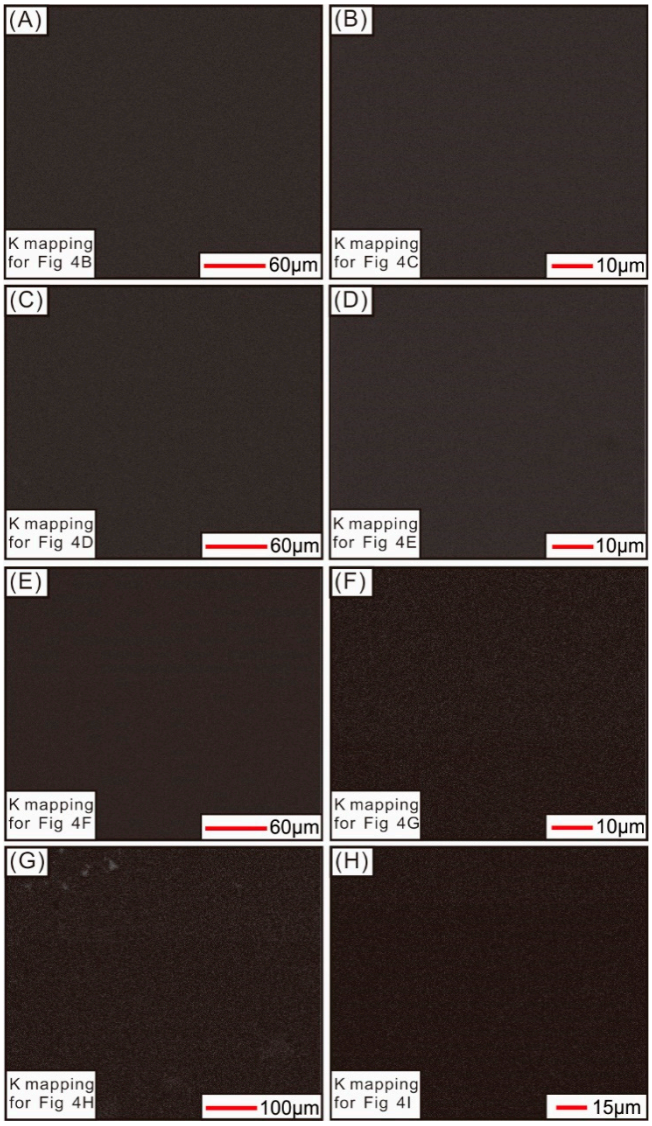

Figure 5. SEM-EDS elemental mapping of potassium (K) for pyrites in Figure 4B–I (**A**–**H**). The mapping results show that the K content of the pyrites is below the detection limit of the instrument, supporting the absence of K-rich inclusion in the pyrites.

4.2. Rb-Sr-Pb-S Isotope Data and Isochron Ages

Pyrite sub-samples from specimen A contain 0.1353–0.1655 ppm Rb and 0.1358–0.1958 ppm Sr and have $^{87}Rb/^{86}Sr$ and $^{87}Sr/^{86}Sr$ ratios of 2.355–3.379 and 0.718340–0.721307, respectively (Table 1), which yield an isochron age of 206 ± 13 Ma (2σ), with an initial $^{87}Sr/^{86}Sr$ ratio (Sr_i) of 0.71138 ± 0.00048 (2σ) (Figure 6A). Pyrite sub-samples from specimen B contain 0.1891–0.2611 ppm Rb and 0.2154–0.2511 ppm Sr (Table 1). An isochron age of 224 ± 28 Ma (2σ) with a Sr_i of 0.7100 ± 0.0011 (2σ) (Figure 6B) is regressed from their $^{87}Rb/^{86}Sr$ and $^{87}Sr/^{86}Sr$ ratios, which are 2.543–3.124 and 0.718049–0.719882, respectively (Table 1). The two Rb-Sr isochrons result in identical ages and Sr_i, within analytical uncertainties, indicating that these ages are not mixing isochron ages, and that the analyzed pyrites were precipitated synchronously.

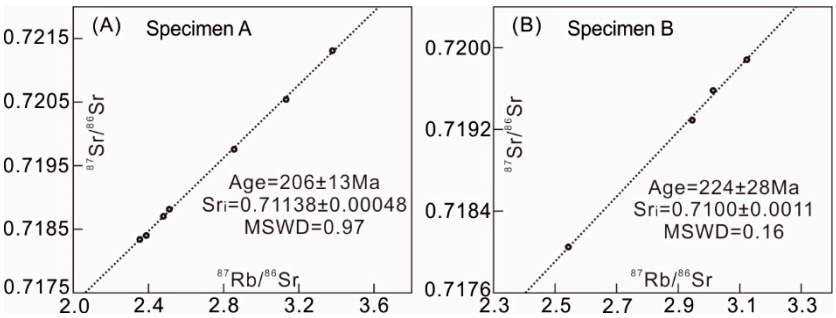

Figure 6. (**A**,**B**): Rubidium-Strontium isochrons of pyrite separates from carbonate rock specimens A and B, respectively, located at ~4952 m in the YD-2 well. (Sr_i represents the initial $^{87}Sr/^{86}Sr$ ratio. MSWD is the mean square of weighted deviates.)

Table 1. Rubidium-Strontium isotope data for pyrite sub-samples from specimens A and B in this study.

Sample	Subsample Analysis	Rb [ppm]	Sr [ppm]	$^{87}Rb/^{86}Sr$	$^{87}Sr/^{86}Sr$	±2σ	* Sr_i
A	A-1	0.1644	0.1420	3.379	0.721307	0.000031	0.711409
	A-2	0.1353	0.1373	2.856	0.719757	0.000033	0.711392
	A-3	0.1459	0.1358	3.133	0.720542	0.000036	0.711365
	A-4	0.1637	0.1890	2.511	0.718813	0.000019	0.711456
	A-5	0.1655	0.1938	2.480	0.718702	0.000029	0.711436
	A-6	0.1580	0.1947	2.355	0.718340	0.000030	0.711442
	A-7	0.1647	0.1958	2.438	0.718401	0.000039	0.711261
B	B-1	0.2251	0.2214	2.946	0.719290	0.000026	0.709903
	B-2	0.2611	0.2511	3.014	0.719580	0.000026	0.709978
	B-3	0.1891	0.2154	2.543	0.718049	0.000024	0.709946
	B-4	0.2383	0.2211	3.124	0.719882	0.000024	0.709931

* Sr_i values were calculated at t = 206 Ma and 224 Ma for specimens A and B, respectively.

Pyrite sub-samples from both specimens have similar Pb isotope ratios. The ratios of $^{206}Pb/^{204}Pb$, $^{207}Pb/^{204}Pb$ and $^{208}Pb/^{204}Pb$ are 18.275–18.972, 15.546–15.712 and 38.245–38.797, respectively (Table 2). $\delta^{34}S$ values of the pyrites range from 31.032‰ to 31.799‰ (Table 3).

Table 2. Lead isotope data for the pyrite sub-samples from specimens A and B in this study.

Sample	Sub-Sample Analysis	$^{206}Pb/^{204}Pb$	±2σ	$^{207}Pb/^{204}Pb$	±2σ	$^{208}Pb/^{204}Pb$	±2σ
A	A-1	18.355	0.006	15.546	0.005	38.245	0.013
	A-2	18.482	0.002	15.672	0.002	38.797	0.005
	A-3	18.361	0.002	15.603	0.001	38.398	0.004
	A-4	18.484	0.003	15.646	0.002	38.493	0.006
	A-5	18.334	0.004	15.616	0.004	38.390	0.008
	A-6	18.363	0.003	15.643	0.003	38.465	0.007
	A-7	18.451	0.003	15.607	0.003	38.418	0.007
B	B-1	18.374	0.003	15.621	0.002	38.413	0.006
	B-2	18.343	0.004	15.618	0.003	38.427	0.008
	B-3	18.275	0.004	15.588	0.003	38.306	0.008
	B-4	18.972	0.004	15.712	0.003	38.711	0.007

Table 3. Sulfur isotope data for the pyrites in this study.

Sample ID	No.	$\delta^{34}S$ (‰)
Specimen A	A	31.624
Specimen A	A-rpt *	31.799
Specimen B	B	31.310
Specimen B	B-rpt	31.032

* rpt denotes replicate analyses.

5. Discussion

5.1. Pyrite Rb-Sr Geochronology: A Robust Dating Technique for Petroleum Systems

In contrast to the Rb-Sr budget in ore-associated pyrite, which is mainly attributed to K-rich inclusions [3,29], Rb and Sr atoms mainly reside in the crystal lattice as inclusions are absent in the studied pyrite (Figure 4). The Rb-Sr data also support the absence of K-rich inclusions: (1) Pyrites in this study have Rb and Sr content generally lower than ore-related pyrites. A compiled Rb-Sr dataset suggests that most (~70%) ore-related pyrite have Rb and Sr content higher than the pyrite samples in this study (Figure 7); (2) randomly-selected sub-samples of each specimen have similar Rb-Sr concentrations (Table 1). This also implies that the Rb and Sr budget in this case cannot be mainly attributed to randomly distributed K-rich inclusions. In addition, the identical ages within analytical uncertainties yielded by Rb-Sr data from the two specimens at the same sampling site also exclude the dominant residence of Rb and Sr atoms in K-rich inclusions.

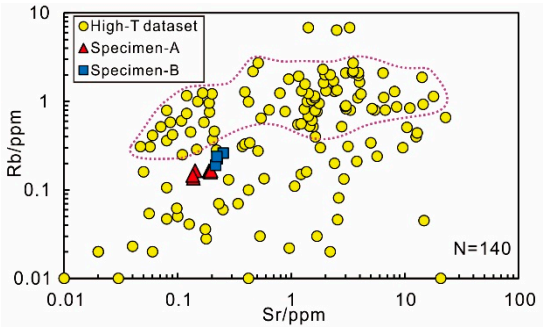

Figure 7. Rb-Sr concentration data are compared between pyrite in this study and pyrite samples in high-temperature ore systems (log-log scale). Rb-Sr data sources: [29–43].

The absence of K-rich inclusions in pyrite suggests that initial Sr isotopic homogenization can be easily attained during the precipitation of pyrite. The obtained Rb-Sr ages for pyrite, thus, should be true isochron ages rather than mixing isochron ages. In addition, closure temperature for the Rb-Sr isotope system in pyrite is estimated between 227 °C and 320 °C [3], which is higher than the temperature for petroleum system events, e.g., 60–100 °C for oil generation [7], below 100 °C for hydrocarbon charge [6], and 100–180 °C for destruction of hydrocarbon reservoirs [7]. This implies that the Rb-Sr geochronometer in pyrite is insensitive to post-precipitation events and difficult to overprint in petroleum systems. Therefore, the Rb-Sr isotopic system in pyrite documents the time of its crystallization. The age data can be further used to constrain petroleum system events by integrating radiogenic (e.g., Pb, Sr) and stable isotopic (e.g., S) analyses of the dated pyrite.

5.2. Source of Metals in Hydrothermal Fluid

Ordovician carbonate rocks intersected by YD-2 were deposited in a marine environment, which is characterized by the general lack of terrigenous input [44]. Therefore, pyrite in the Ordovician reservoir is unlikely to be of detrital origin, but was most likely formed through in-situ precipitation [45]. Hydrothermal fluid is an important carrier of ore metals (e.g., Fe, Pb) [46] and can provide a potential source of iron for the formation of pyrite in carbonate rocks [47,48]. The coexistence of pyrite with other hydrothermal minerals (e.g., calcite, quartz) and the embayment structure between these minerals shown in the photomicrographs (Figure 4A) demonstrate a hydrothermal origin for the pyrites. The hydrothermal origin of these pyrites is also supported by their coeval precipitation ages. The Rb-Sr isochron age of the pyrites, ca. 224–206 Ma, is younger than the depositional age of their host rock (i.e., Ordovician) but approaches the onset of rifting in the Kuqa Depression (Late Triassic), when hydrothermal activity commonly occurred [23].

Metals in hydrothermal fluids from which the pyrites precipitated could have originated from three main repositories, i.e. the mantle, crust, and/or metamorphic basement of the sedimentary basin [49–51]. Lead-strontium isotope compositions of pyrites can provide important constraints on the

sources of metal in fluid systems [33]. A compiled Pb-Sr isotope dataset for these three repositories within or adjacent to the Tarim Basin was employed to constrain the possible metal sources for the hydrothermal fluid (Figure 8).

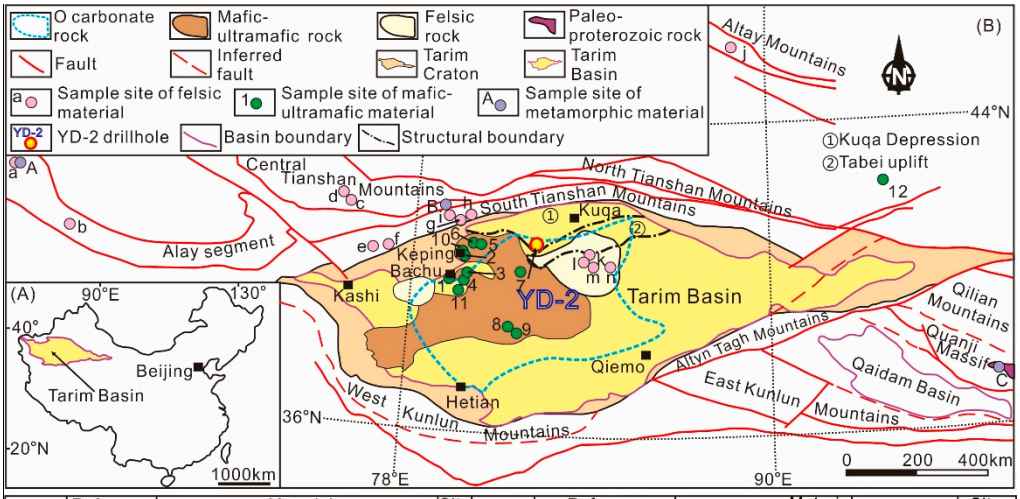

	Reference	Material	Site		Reference	Material	Site
Felsic	Ref[50]	294Ma K-feldspar in granite	g,h	Mafic& ultra-mafic	Ref[52]	275Ma mafic&ultramafic dyke	1
		290Ma K-feldspar in granite	a,c			276Ma basaltic flow	2
		285Ma K-feldspar in granite	b		Ref[53]	290–260Ma basaltic rock	3,4,5, 6,7,8,9
		280Ma K-feldspar in granite	e,f		Ref[54]	292Ma basalt	10
		279Ma K-feldspar in granite	i		Ref[55]	281–275Ma diorite and syenitic rock	11
		180Ma K-feldspar in granite	j		Ref[37]	283Ma mafic-ultramafic intrusion	12
		Upper Paleozoic K-feldspar in granite	d	Metam-orphic	Ref[50]	Є schist	A
	Ref[51]	282–274Ma felsic volcanic rock	k,l, m,n			Ediacaran schist	B
					Ref[56]	1834Ma metamorphosed mafic dyke	C

Figure 8. (**A**): Simplified map showing the location of the Tarim Basin in China; (**B**): A map showing sample sites for Pb and Sr isotope data from published studies used for comparing with Pb-Sr isotope data for pyrites in this study. Є—Cambrian; O—Ordovician; a–n—Sample sites of felsic material (e.g., granite); 1–12—Sample sites of mafic-ultramafic material (e.g., basalt); A–C—Sample sites of metamorphic material (e.g., schist).

As shown in Figure 9A–C, lead-strontium isotopic ratios of the studied pyrites plot in a field that overlaps the areas defined by mafic-ultramafic (e.g., basalt), felsic (e.g., granite), and metamorphic rocks, but show more affinity with the felsic rocks. Lead isotopic ratios also show a mixed source for the pyrites, as the sub-sample analyses are also distributed in the field that overlaps the three repositories on the plots of $^{207}Pb/^{204}Pb$-$^{206}Pb/^{204}Pb$ (Figure 10A) and $^{208}Pb/^{204}Pb$-$^{206}Pb/^{204}Pb$ (Figure 10B). We note that one pyrite sub-sample plots outside the main trend on the Pb-Pb isotope plots (Figure 10), reflecting some Pb isotope heterogeneity.

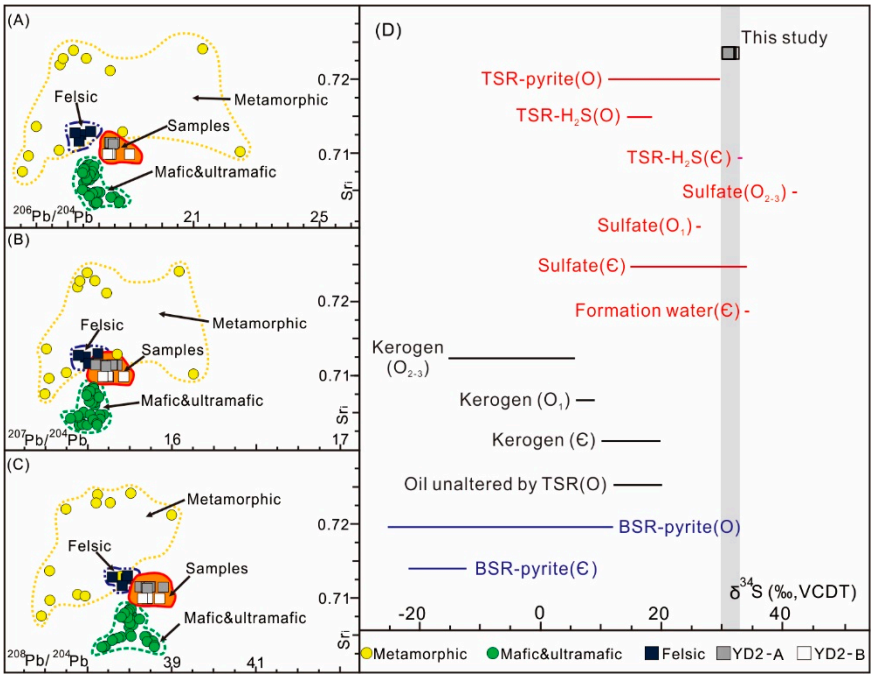

Figure 9. (**A**): Sr_i-$^{206}Pb/^{204}Pb$, (**B**): Sr_i-$^{207}Pb/^{204}Pb$, (**C**): Sr_i-$^{208}Pb/^{204}Pb$ and (**D**): S isotope ratios of the pyrites in this study compared with spatially and temporally associated materials from the literature. Whole-rock Pb isotope ratios were corrected to their initial ratios. Є—Cambrian; O—Ordovician; TSR—thermochemical sulfate reduction; BSR—bacterial sulfate reduction; Sr_i—initial $^{87}Sr/^{86}Sr$ value; VCDT—Vienna Canyon Diablo Troilite. Lead and strontium isotope data sources: (1) felsic rocks: [50,51]; (2) mafic and ultra-mafic rocks: [52–56]; (3) metamorphic rocks: [50,56]. Sulfur isotope data sources: (1) Ordovician BSR-derived pyrites: [14,17–19] ; (2) Ordovician TSR-derived pyrites: [13,15,18,19]; (3) Middle-Upper Ordovician sulfates: [17]; (4) Ordovician TSR-derived H_2S: [57]; (5) Lower Ordovician sulfates: [14]; (6) Lower Ordovician kerogen: [58]; (7) Middle-Upper Ordovician kerogen: [58]; (8) Middle-Upper Ordovician non-degraded oil: [58]; (9) Cambrian BSR-derived pyrites: [16,18]; (10) Cambrian sulfates: [13,14,16,18]; (11) Cambrian formation water: [18]; (12) Cambrian TSR-derived H_2S: [18]; (13) Cambrian kerogen: [58].

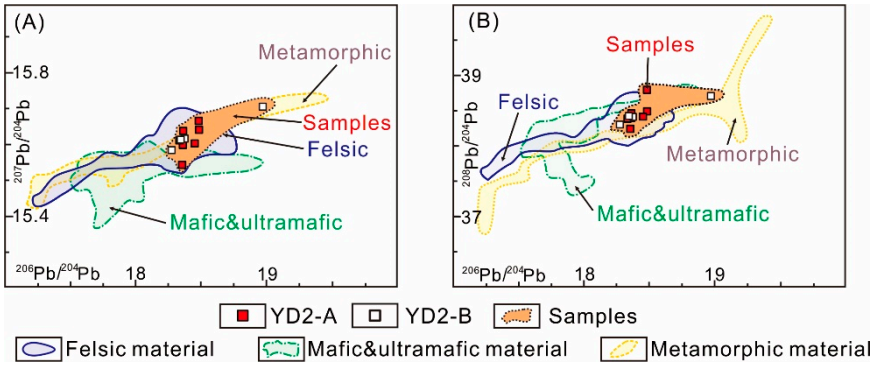

Figure 10. Lead isotope ratios of pyrite sub-samples compared with spatially- and temporally-associated materials ((**A**): $^{207}Pb/^{204}Pb$-$^{206}Pb/^{204}Pb$; (**B**): $^{208}Pb/^{204}Pb$-$^{206}Pb/^{204}Pb$). Lead isotope ratios in (A) and (B) are corrected to their initial ratios. The fields of metamorphic, felsic and mafic-ultramafic are drawn according to lead isotope data of material from the literature. Lead isotope data sources: (1) felsic rocks: [50,51]; (2) mafic and ultra-mafic rocks: [52–55]; (3) metamorphic rocks: [50,56].

5.3. Source of Sulfur

Sulfur in pyrites from carbonate reservoirs can be directly inherited from the thermal degradation of organosulfur compounds in crude oil or obtained from H_2S, which can be generated either through TSR or BSR [47].

Sulfur isotopic composition of pyrites can provide an important constraint on the origin of their sulfur. As shown in Figure 9D, $\delta^{34}S$ values of the pyrites are compared with sulfur isotopic ratios of potential sulfur providers (e.g., kerogen, oil, sulfate, formation water) and products of TSR and BSR (e.g., pyrites, H_2S). The large discrepancy between $\delta^{34}S$ values of pyrites in this study (+31.032‰ to +31.799‰) and kerogen or oil unaltered by TSR (−15.3‰ to +19.4‰ and +11.9‰ to +20.5‰, respectively) precludes the possibility of direct inheritance of sulfur from hydrocarbon precursors (Figure 9D). The pyrites are also unlikely to have been precipitated via BSR processes because their $\delta^{34}S$ values are more enriched than those of BSR-derived pyrites, which have depleted $\delta^{34}S$ values ranging from −25.7‰ to −11.6‰ (Figure 9D). Instead, the similarity in $\delta^{34}S$ values between the studied pyrites and pyrites (+11.200‰ to +29.700‰) and H_2S (+14.210‰ to +33.000‰) that are produced by TSR processes in the Tarim Basin indicates that the pyrites from YD-2 most likely are by-products of TSR. Furthermore, the TSR origin is also supported by the insignificant sulfur isotopic fractionation between pyrites and sulfates ($\delta^{34}S_{sulfate}$ = +14.840‰ − 42.100‰), especially those in Ordovician strata ($\delta^{34}S_{sulfate}$ = +24.460‰ − 42.100‰) (Figure 9D), because TSR results in less sulfur isotopic fractionation between sulfates and pyrites when compared with those in BSR [7].

TSR requires the presence of both sulfates (either as minerals or dissolved in formation water) and hydrocarbons, as well as a relative high temperature (100–180 °C) [7]. Several lines of evidence support that TSR might have taken place in the Ordovician reservoir intersected by the YD-2 well: (1) Both the industrial discovery (i.e., heavy oil flows) and evidence from photomicrographs of the samples (e.g., solid bitumen in Figure 3B) imply that there should have been sufficient reactive hydrocarbons for sulfate reduction to occur; (2) Anhydrite was identified in the Ordovician strata at ~4950.1 m in the YD-2 well (i.e., ~1.9 m above the sampling depth) (Figure 2A) [22], which may have been the SO_4^{2-} source for the TSR; and (3) A case study of fluid inclusions hosted by hydrothermal minerals (e.g., calcite) from the Ordovician carbonate reservoir in the northern Tarim Basin suggests that the temperature of hydrothermal fluids in this region was higher than 154 °C, which can facilitate TSR [20]. In addition, petroleum recovered from the studied area has more enriched carbon isotopic compositions ($\delta^{13}C$ = −25‰ − −28‰, [59]) compared to ordinary Ordovician-hosted petroleum ($\delta^{13}C$ = −31‰ − −33‰, [21]), indicating that petroleum has likely been oxidized by TSR because the increase of temperature results in the enrichment in carbon isotopic compositions of petroleum [21].

5.4. Timing of Alteration of the Paleo-Oil Pool

The wide distribution of hydrothermal minerals in Ordovician hydrocarbon reservoirs indicates the common occurrence of hydrothermal activities in the Tarim Basin [48]. The hydrothermal mineral assemblage of pyrite + calcite + quartz is also present in samples in this study (Figure 4A). Previous studies have indicated that migrated hydrocarbons can be altered by hydrothermal fluid in three aspects: (1) modifying the molecular composition of hydrocarbons, e.g., generating typical biomarkers of combustion; (2) the preferential loss of components depleted in carbon isotopic compositions; and (3) facilitating the TSR by providing a high temperature environment [21].

Although hydrothermal activities and their influence on hydrocarbons have been well documented, their absolute timing is poorly constrained. This study obtained Rb-Sr isochron ages of ca. 224–206 Ma, indicating that the pyrites precipitated from hydrothermal fluid associated with Late Triassic rifting in the Kuqa Depression, and not early Permian magmatism, as previously proposed [20]. The pyrite Rb-Sr geochronological evidence is consistent with the lack of early Permian magmatic records in the region, since few Permian magmatic rocks have been identified in the Yudong area, suggesting that any thermal influence of early Permian magmatism was insignificant [49].

As discussed in the preceding sections, the studied pyrites are also indicators of the TSR process. Therefore, Rb-Sr isochron ages of pyrite may also record the timing of TSR alteration of the paleo-oil

pool if hydrothermal activity and TSR occur contemporaneously. Burial history analysis indicates that there was regional uplift during the late Permian to Middle Triassic in the Kuqa Depression [23]. Hydrogen sulfide generated prior to the uplifting event could have potentially leaked from the Ordovician reservoir due to erosion of the caprocks. Therefore, hydrogen sulfide precursors of the pyrites may have been generated after the Middle Triassic. Considering the Late Triassic precipitation age of the pyrites, it is reasonable to deduce that both the hydrothermal activity and TSR occurred at ca. 224–206 Ma. Hydrothermal fluid flow can result in a high-temperature environment, which is essential for the TSR. Thus, we propose that hydrothermal activity was a key factor in triggering the TSR in the Ordovician reservoirs of the Yudong region.

6. Conclusions

This is the first study to integrate the low-blank and high-sensitive Rb-Sr ID-TIMS dating technique with Pb-S isotope analysis for direct dating and characterizing key events in petroleum systems using small pyrite samples (2–6 mg). Through applying this method to samples taken from an Ordovician carbonate reservoir in the Yudong region of the Kuqa Depression, northern Tarim Basin, the timing of hydrothermally-triggered TSR alteration of a paleo-oil pool is established at ca. 224–206 Ma. SEM investigations demonstrate that Rb and Sr atoms mainly reside in the crystal lattice of the pyrites because neither fluid nor mineral inclusions are found in the pyrites. The rigorous Rb-Sr isochron relations documented by the samples indicate that such residency can result in sufficient Rb/Sr fractionation and initial Sr isotopic homogenization for constructing an isochron. In addition, the closure temperature (227–320 °C) for the Rb-Sr isotope system in pyrite is estimated to be higher than the precipitation temperature for pyrite in the petroleum-related environment (below 200 °C), suggesting that the Rb-Sr age for pyrite was not overprinted by post-precipitation alterations. This study, therefore, confirms that Rb-Sr pyrite geochronology is potentially an important tool for constraining petroleum system events. Besides obtaining reliable isotopic ages, the determination of stable (e.g., S) and radiogenic (e.g., Sr and Pb) isotopic ratios of pyrites can also lead to a better understanding of petroleum systems. The applicability of this geochronometer to petroleum system analysis could be enhanced by in-situ analyses of Fe-S isotopes and trace elements (e.g., transition metals, such as molybdenum and zinc) of pyrite, which can provide additional constraints on its origin and precipitation environment.

Author Contributions: Conceptualization, X.-C.W; methodology, C.-F.L.; software, S.L.; validation, S.L., X.-C.W. and C.-F.L.; formal analysis, S.L.; investigation, S.L. and S.-Y.H.; resources, K.L., L.G., J.L. and L.W.; data curation, S.L. and S.-Y.H.; writing—original draft preparation, S.L.; writing—review and editing, X.-C.W, S.A.W. and K.L.; visualization, S.L. and L.W..; supervision, X.-C.W.; project administration, X.-C.W.; funding acquisition, X.-C.W. and K.L. All authors have read and agreed to the published version of the manuscript.

Funding: This work was supported by the Research Start-up Project for Introduced Talent of Yunnan University (No. 20190043), the SINOPEC Key Laboratory on Hydrocarbon Accumulation (No. 33550007-17-ZC0613-0031), the Chinese National Major Petroleum Project of China (No. 2011ZX05006), and the Strategic Priority Research Program of the Chinese Academy of Sciences (Grant No. XDA14010401).

Acknowledgments: We thank the academic editor and three anonymous reviewers for their constructive suggestions and comments. Lian-Jun Feng (Institute of Geology and Geophysics, CAS, Beijing) is thanked for sulfur isotope analyses. We also thank Fred Jourdan (Curtin University) for constructive suggestions on the selection of dating methods for pyrites.

Conflicts of Interest: The authors declare no conflict of interest.

References

1. Georgiev, S.V.; Stein, H.J.; Hannah, J.L.; Galimberti, R.; Nali, M.; Yang, G.; Zimmerman, A. Re–Os dating of maltenes and asphaltenes within single samples of crude oil. *Geochim. Cosmochim. Acta* **2016**, *179*, 53–75.
2. Li, S.; Wang, X.-C.; Li, C.-F.; Wilde, S.A.; Zhang, Y.; Golding, S.D.; Liu, K.; Zhang, Y. Direct Rubidium-Strontium Dating of Hydrocarbon Charge Using Small Authigenic Illitic Clay Aliquots from the Silurian Bituminous Sandstone in the Tarim Basin, NW China. *Sci. Rep.* **2019**, *9*, 1–13.

3. Yang, J.; Zhou, X. The Rb-Sr isochron of ore and pyrite sub-samples from Linglong gold deposit, Jiaodong Peninsula, eastern China and their geological significance. *Chin. Sci. Bull.* **2000**, *45*, 2272–2277.
4. Berner, R.A. Sedimentary pyrite formation: An update. *Geochim. Cosmochim. Acta* **1984**, *48*, 605–615.
5. Rasmussen, B. Evidence for pervasive petroleum generation and migration in 3.2 and 2.63 Ga shales. *Geology* **2005**, *33*, 497–500.
6. Ellis, G. Hydrocarbon Entrapment in Triassic to Late Jurassic Reservoirs in the Timor Sea, Australia—New Insights. *APPEA J.* **2007**, *47*, 39–53.
7. Machel, H.G.; Krouse, H.R.; Sassen, R. Products and distinguishing criteria of bacterial and thermochemical sulfate reduction. *Appl. Geochem.* **1995**, *10*, 373–389.
8. Large, R.R.; Danyushevsky, L.; Hollitt, C.; Maslennikov, V.; Meffre, S.; Gilbert, S.; Bull, S.; Scott, R.; Emsbo, P.; Thomas, H.; et al. Gold and Trace Element Zonation in Pyrite Using a Laser Imaging Technique: Implications for the Timing of Gold in Orogenic and Carlin-Style Sediment-Hosted Deposits. *Econ. Geol.* **2009**, *104*, 635–668.
9. Large, R.R.; Halpin, J.A.; Danyushevsky, L.; Maslennikov, V.V.; Bull, S.W.; Long, J.A.; Gregory, D.D.; Lounejeva, E.; Lyons, T.W.; Sack, P.J.; et al. Trace element content of sedimentary pyrite as a new proxy for deep-time ocean–atmosphere evolution. *Earth Planet. Sci. Lett.* **2014**, *389*, 209–220.
10. Reich, M.; Deditius, A.; Chryssoulis, S.; Li, J.-W.; Ma, C.-Q.; Parada, M.-A.; Barra, F.; Mittermayr, F. Pyrite as a record of hydrothermal fluid evolution in a porphyry copper system: A SIMS/EMPA trace element study. *Geochim. Cosmochim. Acta* **2013**, *104*, 42–62.
11. Li, J.; Wang, X.-C.; Xu, J.-F.; Xu, Y.-G.; Tang, G.-J.; Wang, Q. Disequilibrium-induced initial Os isotopic heterogeneity in gram aliquots of single basaltic rock powders: Implications for dating and source tracing. *Chem. Geol.* **2015**, *406*, 10–17.
12. Li, C.; Chu, Z.-Y.; Guo, J.-H.; Li, Y.-L.; Yang, Y.-H.; Li, X.-H. A rapid single column separation scheme for high-precision Sr–Nd–Pb isotopic analysis in geological samples using thermal ionization mass spectrometry. *Anal. Methods* **2015**, *7*, 4793–4802.
13. Cai, C.; Hu, W.; Worden, R.H. Thermochemical sulphate reduction in Cambro–Ordovician carbonates in Central Tarim. *Mar. Pet. Geol.* **2001**, *18*, 729–741.
14. Cai, C.; Worden, R.H.; Wang, Q.; Xiang, T.; Zhu, J.; Chu, X. Chemical and isotopic evidence for secondary alteration of natural gases in the Hetianhe Field, Bachu Uplift of the Tarim Basin. *Org. Geochem.* **2002**, *33*, 1415–1427.
15. Cai, C.; Li, K.; Anlai, M.; Zhang, C.; Xu, Z.; Worden, R.H.; Wu, G.; Zhang, B.; Chen, L. Distinguishing Cambrian from Upper Ordovician source rocks: Evidence from sulfur isotopes and biomarkers in the Tarim Basin. *Org. Geochem.* **2009**, *40*, 755–768.
16. Li, S.; Shi, Q.; Pang, X.; Zhang, B.; Zhang, H. Origin of the unusually high dibenzothiophene oils in Tazhong-4 Oilfield of Tarim Basin and its implication in deep petroleum exploration. *Org. Geochem.* **2012**, *48*, 56–80.
17. Lü, X.; Xie, Q.; Yang, N.; Li, J. Hydrocarbon accumulation in deep fluid modified carbonate rock in the Tarim Basin. *Chin. Sci. Bull.* **2007**, *52*, 184–192.
18. Jia, L.; Cai, C.; Yang, H.; Li, H.; Wang, T.; Zhang, B.; Jiang, L.; Tao, X. Thermochemical and bacterial sulfate reduction in the Cambrian and Lower Ordovician carbonates in the Tazhong Area, Tarim Basin, NW China: Evidence from fluid inclusions, C, S, and Sr isotopic data. *Geofluids* **2014**, *15*, 421–437.
19. Zhu, D.-Y.; Meng, Q.-Q. Genesis of pyrite in Ordovician carbonate of the Tarim Basin. *Acta Petrol. Mineral.* **2010**, *29*, 516–524.
20. Li, K.; Cai, C.; He, H.; Jiang, L.; Cai, L.; Xiang, L.; Huang, S.; Zhang, C. Origin of palaeo-waters in the Ordovician carbonates in Tahe oilfield, Tarim Basin: Constraints from fluid inclusions and Sr, C and O isotopes. *Geofluids* **2010**, *11*, 71–86.
21. Huang, H.; Zhang, S.; Su, J. Palaeozoic oil–source correlation in the Tarim Basin, NW China: A review. *Org. Geochem.* **2016**, *94*, 32–46.
22. Zhou, J.-F.; Zhang, H.-Q.; Yu, J.-P.; Zhu, Y.-F.; Yao, Q.-Z.; Yuan, Y-C. Analysis of the Hydrocarbon Accumulation Conditions and Exploration Potential in the Ordovician in Yudong Area of West Tabei Uplift. *Nat. Gas Geosci.* **2015**, *26*, 121–129.
23. Liu, J.; Jiang, Z.; Liu, K.; Gui, L.; Xing, J. Hydrocarbon sources and charge history in the Southern Slope Region, Kuqa Foreland Basin, northwestern China. *Mar. Pet. Geol.* **2016**, *74*, 26–46.

24. Jia, C.; Wei, G. Structural characteristics and petroliferous features of Tarim Basin. *Chin. Sci. Bull.* **2002**, *47*, 1–11.
25. Li, C.-F.; Guo, J.-H.; Chu, Z.-Y.; Feng, L.-J.; Wang, X.-C. Direct High-Precision Measurements of the 87Sr/86Sr Isotope Ratio in Natural Water without Chemical Separation Using Thermal Ionization Mass Spectrometry Equipped with 1012 Ω Resistors. *Anal. Chem.* **2015**, *87*, 7426–7432.
26. Pin, C.; Gannoun, A.; Dupont, A. Rapid, simultaneous separation of Sr, Pb, and Nd by extraction chromatography prior to isotope ratios determination by TIMS and MC-ICP-MS. *J. Anal. At. Spectrom.***2014**, *29*, 1858–1870.
27. Ludwig, K. *User's Manual for Isoplot 3.00: A Geochronological Toolkit for Microsoft Excel*; Geochronology Center: Berkeley, CA, USA, 2003.
28. Steiger, R.H.; Jäger, E. Subcommission on geochronology: Convention on the use of decay constants in geo- and cosmochronology. *Earth Planet. Sci. Lett.* **1977**, *36*, 359–362.
29. Li, Q.-L.; Chen, F.; Yang, J.-H.; Fan, H.-R. Single grain pyrite Rb–Sr dating of the Linglong gold deposit, eastern China. *Ore Geol. Rev.* **2008**, *34*, 263–270.
30. Yang, J.-H.; Zhou, X.-H. Rb-Sr, Sm-Nd, and Pb isotope systematics of pyrite: Implications for the age and genesis of lode gold deposits. *Geology* **2001**, *29*, 711–714.
31. Cao, H.-W.; Zhang, S.-T.; Santosh, M.; Zheng, L.; Tang, L.; Li, D.; Zhang, X.-H.; Zhang, Y.-H. The Luanchuan Mo–W–Pb–Zn–Ag magmatic–hydrothermal system in the East Qinling metallogenic belt, China: Constrains on metallogenesis from C–H–O–S–Pb isotope compositions and Rb–Sr isochron ages. *J. Asian Earth Sci.* **2015**, *111*, 751–780.
32. Dong, L.; Wan, B.; Yang, W.; Deng, C.; Chen, Z.; Yang, L.; Cai, K.; Xiao, W. Rb-Sr geochronology of single gold-bearing pyrite grains from the Katbasu gold deposit in the South Tianshan, China and its geological significance. *Ore Geol. Rev.* **2018**, *100*, 99–110.
33. Han, Y.; Li, X.; Zhang, S.; Zhang, Y.; Chen, F. Single grain Rb-Sr dating of euhedral and cataclastic pyrite from the Qiyugou gold deposit in western Henan, central China. *Chin. Sci. Bull.* **2007**, *52*, 1820–1826.
34. Hu, Q.; Wang, Y.; Mao, J.; Wei, R.; Liu, S.; Ye, D.; Yuan, Q.; Dou, P.; Qiaoqing, H.; Yitian, W.; et al. Timing of the formation of the Changba–Lijiagou Pb–Zn ore deposit, Gansu Province, China: Evidence from Rb–Sr isotopic dating of sulfides. *J. Asian Earth Sci.* **2015**, *103*, 350–359.
35. Ni, Z.-Y.; Chen, Y.-J.; Li, N.; Zhang, H. Pb–Sr–Nd isotope constraints on the fluid source of the Dahu Au–Mo deposit in Qinling Orogen, central China, and implication for Triassic tectonic setting. *Ore Geol. Rev.* **2012**, *46*, 60–67.
36. Vadlamani, R.; Golani, P.R. Rb-Sr direct dating of pyrite from the Pipela VMS Zn-Cu prospect, Rajasthan, NW India. *J. Geol. Soc. India* **2011**, *77*, 149–159.
37. Sun, W.-Y.; Li, S.-R.; Santosh, M.; Wang, X.; Zhang, L.-J. Isotope geochemistry and geochronology of the Qiubudong silver deposit, central North China Craton: Implications for ore genesis and lithospheric dynamics. *Ore Geol. Rev.* **2014**, *57*, 229–242.
38. Wang, C.; Deng, J.; Santosh, M.; Carranza, E.J.M.; Gong, Q.; Guo, C.; Xia, R.; Lai, X. Timing, tectonic implications and genesis of gold mineralization in the Xincheng gold deposit, China: C–H–O isotopes, pyrite Rb–Sr and zircon fission track thermochronometry. *Ore Geol. Rev.* **2015**, *65*, 659–673.
39. Wang, Y.; Zeng, Q.; Liu, J. Rb-Sr Dating of Gold-bearing Pyrites from Wulaga Gold Deposit and its Geological Significance. *Resour. Geol.* **2014**, *64*, 262–270.
40. Yao, J.; Hua, R.; Lin, J. REE, Pb-S isotope geochemistry, and Rb-Sr isochron age of pyrites in the Baoshan deposit, south Hunan province, China. *Acta Geol. Sin.* **2006**, *80*, 1045–1054.
41. Zhang, L. 40Ar/39Ar and Rb-Sr isochron dating of the gold deposits on northern margin of the Jiaolai Basin, Shandong, China. *Sci. China Ser. D: Earth Sci.* **2003**, *46*, 708–718.
42. Zhao, X.-F.; Zhou, M.-F.; Li, J.-W.; Selby, D.; Li, X.-H.; Qi, L. Sulfide Re-os and Rb-sr isotope dating of the kangdian IOCG metallogenic province, southwest china: Implications for regional metallogenesis. *Econ. Geol.* **2013**, *108*, 1489–1498.
43. Zhou, J.; Huang, Z.; Zhou, M.; Li, X.; Jin, Z. Constraints of C–O–S–Pb isotope compositions and Rb–Sr isotopic age on the origin of the Tianqiao carbonate-hosted Pb–Zn deposit, SW China. *Ore Geol. Rev.* **2013**, *53*, 77–92.
44. Zhang, S.; Huang, H. Geochemistry of Palaeozoic marine petroleum from the Tarim Basin, NW China: Part 1. Oil family classification. *Org. Geochem.* **2005**, *36*, 1204–1214.

45. Riciputi, L.R.; Cole, D.R.; Machel, H.G. Sulfide formation in reservoir carbonates of the Devonian Nisku Formation, Alberta, Canada: An ion microprobe study. *Geochim. Cosmochim. Acta* **1996**, *60*, 325–336.
46. Hedenquist, J.W.; Lowenstern, J.B. The role of magmas in the formation of hydrothermal ore deposits. *Nature* **1994**, *370*, 519–527.
47. Worden, R.; Smalley, P. H2S-producing reactions in deep carbonate gas reservoirs: Khuff Formation, Abu Dhabi. *Chem. Geol.* **1996**, *133*, 157–171.
48. Cai, C.; Li, K.; Li, H.; Zhang, B. Evidence for cross formational hot brine flow from integrated 87Sr/86Sr, REE and fluid inclusions of the Ordovician veins in Central Tarim, China. *Appl. Geochem.* **2008**, *23*, 2226–2235.
49. Xu, Y.-G.; Wei, X.; Luo, Z.-Y.; Liu, H.-Q.; Cao, J. The Early Permian Tarim Large Igneous Province: Main characteristics and a plume incubation model. *Lithos* **2014**, *204*, 20–35.
50. Chiaradia, M.; Konopelko, D.; Seltmann, R.; Cliff, R.A. Lead isotope variations across terrane boundaries of the Tien Shan and Chinese Altay. *Miner. Deposita* **2006**, *41*, 411–428.
51. Yu, J.; Mo, X.; Dong, G.; Yu, X.; Xing, F.; Li, Y.; Huang, X. 2011. Felsic volcanic rocks from northern Tarim, NW China: Zircon U-Pb dating and geochemical characteristics. *Acta Petrol. Sin*. **2011**, *27*, 2184-2194.
52. Zhou, M.-F.; Zhao, J.-H.; Jiang, C.-Y.; Gao, J.-F.; Wang, W.; Yang, S.-H. OIB-like, heterogeneous mantle sources of Permian basaltic magmatism in the western Tarim Basin, NW China: Implications for a possible Permian large igneous province. *Lithos* **2009**, *113*, 583–594.
53. Zhang, Y.; Liu, J.; Guo, Z. Permian basaltic rocks in the Tarim basin, NW China: Implications for plume–lithosphere interaction. *Gondwana Res.* **2010**, *18*, 596–610.
54. Zhang, D.; Zhou, T.; Yuan, F.; Jowitt, S.M.; Fan, Y.; Liu, S. Source, evolution and emplacement of Permian Tarim Basalts: Evidence from U–Pb dating, Sr–Nd–Pb–Hf isotope systematics and whole rock geochemistry of basalts from the Keping area, Xinjiang Uygur Autonomous region, northwest China. *J. Asian Earth Sci.* **2012**, *49*, 175–190.
55. Zou, S.-Y.; Li, Z.-L.; Song, B.; Ernst, R.E.; Li, Y.-Q.; Ren, Z.-Y.; Yang, S.-F.; Chen, H.-L.; Xu, Y.-G.; Song, X.-Y. Zircon U–Pb dating, geochemistry and Sr–Nd–Pb–Hf isotopes of the Wajilitag alkali mafic dikes, and associated diorite and syenitic rocks: Implications for magmatic evolution of the Tarim large igneous province. *Lithos* **2015**, *212*, 428–442.
56. Liao, F.; Zhang, L.; Chen, N.; Sun, M.; Santosh, M.; Wang, Q.; Mustafa, H.A. Geochronology and geochemistry of meta-mafic dykes in the Quanji Massif, NW China: Paleoproterozoic evolution of the Tarim Craton and implications for the assembly of the Columbia supercontinent. *Precambrian Res.* **2014**, *249*, 33–56.
57. Zhu, G.; Zhang, B.; Yang, H.; Su, J.; Han, J. Origin of deep strata gas of Tazhong in Tarim Basin, China. *Org. Geochem.* **2014**, *74*, 85–97.
58. Cai, C.; Zhang, C.; Cai, L.; Wu, G.; Jiang, L.; Xu, Z.; Li, K.; Ma, A.; Chen, L. Origins of Palaeozoic oils in the Tarim Basin: Evidence from sulfur isotopes and biomarkers. *Chem. Geol.* **2009**, *268*, 197–210.
59. Chen, J.; Xiao, Z.; Zhang, S.; Liang, D. Geochemical features and classification of crude oil in the Kuqa Depression, Tarim Basin. Bulletin of Mineralogy. *Petrol. Geochem.* **2005**, *24*, 369.